ACS APPLIED MATERIALS & INTERFACES

Research Article

www.acsami.org

Postsynthetic Functionalization of Mg-MOF-74 with Tetraethylenepentamine: Structural Characterization and Enhanced CO_2 Adsorption

Xiao Su,[†] Lev Bromberg,[†] Vladimir Martis,[‡] Fritz Simeon,[†] Ashfia Huq,[§] and T. Alan Hatton*,[†]

[†]Department of Chemical Engineering, Massachusetts Institute of Technology, Cambridge, Massachusetts 02139, United States

[‡]Surface Measurements Systems, London HA0 4PE, United Kingdom

[§]Chemical and Engineering Materials Division, Oak Ridge National Laboratory, Oak Ridge, Tennessee 37831, United States

Supporting Information

ABSTRACT: Postsynthetic functionalization of magnesium 2,5-dihydroxyterephthalate (Mg-MOF-74) with tetraethylenepentamine (TEPA) resulted in improved CO_2 adsorption performance under dry and humid conditions. XPS, elemental analysis, and neutron powder diffraction studies indicated that TEPA was incorporated throughout the MOF particle, although it coordinated preferentially with the unsaturated metal sites located in the immediate proximity to the surface. Neutron and X-ray powder diffraction analyses showed that the MOF structure was preserved after amine incorporation, with slight changes in the lattice parameters. The adsorption capacity of the functionalized amino-Mg-MOF-74 (TEPA-MOF) for CO_2 was as high as 26.9 wt % versus 23.4 wt % for the original MOF due to the extra binding sites provided by the multiunit amines. The degree of functionalization with the amines was found to be important in enhancing CO_2 adsorption, as the optimal surface coverage improved performance and stability under both pure CO_2 and CO_2/H_2O coadsorption, and with partially saturated surface coverage, optimal CO_2 capacity could be achieved under both wet and dry conditions by a synergistic binding of CO_2 to the amines as well as metal centers.

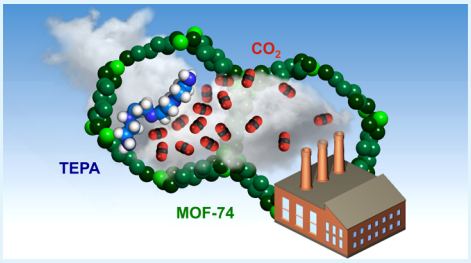

KEYWORDS: *metal−organic framework, magnesium 2,5-dihydroxyterephthalate, amine functionalization, carbon dioxide adsorption, dynamic vapor sorption*

INTRODUCTION

Mitigation of anthropogenic carbon emissions is one of the crucial challenges of the 21st century,[1] as atmospheric accumulation of carbon dioxide affects global warming and results in ocean acidification and related environmental problems.[2,3] Significant effort has been expended on the development of materials for CO_2 capture and removal from process streams and flue gases.[4] These materials include porous adsorbents, which are solid-state alternatives to the well-known amine scrubbing technologies for CO_2 capture and sequestration;[5] they have lower energetic costs, greater environmental sustainability, and regenerability. Adsorption processes can be operated in either the pressure or temperature swing mode, or in conjunction with membrane systems.[6,7] A well-known class of such adsorbents is the set of metal−organic frameworks (MOFs) composed of organic linkers coordinated with metal ions to form open-framework structures that rank among materials with the highest surface areas currently available,[8−10] and, hence, offer great potential for gas-phase separations and storage.[8,11]

Magnesium 2,5-dihydroxyterephthalate (Mg-MOF-74) is an especially attractive MOF for carbon dioxide capture due to its very high dynamic and equilibrium CO_2 uptake, favorable structural characteristics, higher surface areas than those of zeolites, ease of synthesis, and favorable reagents cost.[12,13] The large density of unsaturated magnesium centers and cylindrical pore structure contribute to the strong binding and large uptake of CO_2, imbuing this solid-state adsorbent with one of the highest known ambient temperature (25 °C) capacities (~5 mmol/g at 0.1 bar to ~8 mmol/g at 1 bar CO_2).[13,14] In Mg-MOF-74, the Mg^{2+} ions coordinate the oxygens of the carboxylate and hydroxyl groups of the ligands, with five oxygen atoms and an additional solvent molecule forming the metal coordination sphere.[6] Upon thermal or vacuum activation, the solvent molecule is removed to leave an open binding site available for coordination with another guest molecule, e.g., CO_2, ethylene, or amines (Scheme 1). In addition, MOF-74 can be readily constructed into the thin layer and mixed membrane structures for various postcombustion treatments.[9,15] Beyond MOFs, Mg-based porous materials have shown great promise for CO_2 capture with recently developed Mg-based alkali-modified metal oxide nanoparticles with very high uptakes (from 10.2 up to 15.7 mmol/g) at elevated temperatures.[16,17] Magnesium provides an exceptional Lewis

Received: February 19, 2017
Accepted: February 28, 2017
Published: February 28, 2017

DOI: 10.1021/acsami.7b02471
ACS Appl. Mater. Interfaces 2017, 9, 11299−11306

Scheme 1. Activation of the Mg-Center of Mg-MOF-74 and Subsequent Coordination with Guest Molecule[a]

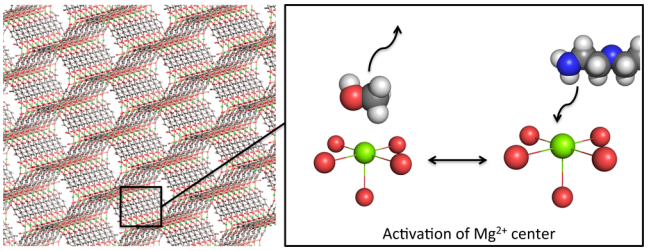

[a]Mg atoms are illustrated in green, and oxygens are in red, with carbons in black and hydrogens in white. The scheme shows the ligand exchange of a bound methanol with a coordinating amine ligand.

acid site with a strong affinity for CO_2 as a conjugate base,[18] and the adsorption capacity of Mg-based MOF-74 is high because the pore structure ensures access to all the metal centers in this material.[12,19]

Postsynthetic functionalization can impart properties to the MOFs that are not attainable by direct synthesis.[20−22] Numerous functionalization methods have been reported, ranging from "click" chemistry to pore impregnation.[21,23,24] For example, encapsulation of active species within the MOF pores by impregnation enables preservation of the MOF morphology while enhancing adsorption properties, especially for CO_2 capture. Postsynthetic functionalization has also been a technique applied in the field of heterogeneous catalysis.[25−29] The inclusion of catalytic groups, for instance, can increase vapor sorption capacities through a reactive adsorption mechanism that both captures and detoxifies volatile organic compounds (VOCs).[30,31] The high porosity of the MOFs can be exploited to construct interconnected polymer/MOF hybrids for heterogeneous catalysis of biomass conversion.[32] Postsynthetic functionalization of MOFs by impregnation with amines can improve the CO_2 adsorption capacity under dilute CO_2 concentrations due to the high amine−CO_2 reaction equilibrium constants.[33−35] In the high CO_2 pressure ranges, the total adsorption capacity of the amino-modified MOFs is typically lower than that of the parent MOFs due to the diminished total surface area after the amine modification.[32,36]

Functionalization of magnesium-based MOFs with ethylenediamine (EDA) has been shown to provide not only enhanced CO_2 binding under dilute concentrations, but also an improved stability under thermal swing operations, relative to the unmodified MOF.[34,35] Previous reports with diamines have shown an increase in the selectivity and augmented kinetics for gas mixtures in low carbon dioxide pressure ranges, with efficient regeneration capabilities.[27] It is important to note, however, that while the stoichiometric binding of an EDA molecule to an unsaturated Mg^{2+} center results in a stronger CO_2 binding, the overall uptake capacity is not improved significantly over that of the unmodified MOF. It has been shown that the amines (both bound and free pendant) can play an important role in coordinating with CO_2 and enhancing energy-efficiency of the system by reducing the temperature swing window.[29] Another challenge in amine functionalization is pore accessibility control, since an excessive number of amino groups tends to crowd the pores and form amine−amine aggregates, hindering transport of CO_2 and ultimately diminishing the uptake capacity of the MOF.[37]

The chemical stability of the MOF structure toward extraneous molecules such as water can also be enhanced by modification with amines.[34,35] This is an important issue for CO_2 capture technologies as most postcombustion flue gases are humid, with exact compositions highly variable depending on the operating conditions at a specific plant, but ranging from 12%CO_2/6%H_2O (~2:1 v/v) in coal-fired plants to ~8%CO_2/15%H_2O (~1:2 v/v) in gas-fired plants.[38,39] Humidity presents a significant challenge for the porous coordination adsorbents as water hydrolyzes the acid−base bridging between the ligand and the metal centers.[40] Stability enhancement in the presence of water has been attributed to masking of the coordinatively unsaturated hydrophilic metal sites by the linked amino groups, while the alkyl groups such as ethylene bridges in EDA imparted hydrophobicity to the MOF structure, thus minimizing water absorption and dissociation of the coordination bonds.[27] In the present work, we hypothesized that longer alkyl groups such as tetraethylene would resist deleterious effects of water even more effectively.

Utilization of alkylamines with multiple amino groups can also be expected to result in an increased total CO_2 capacity of Mg-based MOFs by providing additional pendant adsorption sites beyond the "docking" groups coordinated with the metal center. Multiunit aminoimines (similar to poly(ethylene imines)) have been shown to lead to high carbon dioxide uptake capacity as well as regenerability over multiple cycles.[4] Polyamines can dramatically increase CO_2 capacities of porous carbon materials beyond their inherent values, up to 12-fold in many cases,[41] and the judicious selection of the number of repeating units is important in maintaining a balance between filling pore volume and improving uptake capacity. We impregnated Mg-MOF-74 with tetraethylenepentamine (TEPA) and investigated both the structure of the functionalized MOF and its CO_2 adsorption properties. We selected TEPA as the ligand as it has a maximum diameter of ~13 Å, comparable to the Mg-MOF-74 pore opening median size of 11 Å.

In this work, we investigate the changes in CO_2 adsorption capacity under dry and humid conditions, and MOF stability under humid conditions, when the MOF is functionalized with multiunit amines. We primarily address relative capacity changes imparted by the MOF modification by amines. We combine X-ray and neutron diffraction methods with detailed spectroscopic analysis for a full structural characterization of the functionalized particles, and investigate the distribution of the amine ligands between the surface layers and the bulk of the MOF crystal. TEPA functionalization in this work, in contrast to most published diamine functionalization studies,[32] is shown to enhance the CO_2 uptake capacity significantly (>18% increase) over the CO_2 pressure range from 0.1 to 1 bar under optimal loading conditions. In addition, our work draws attention to the importance of understanding the structural partitioning of a molecular guest within the microporous MOF particles, and is expected to contribute toward further molecular design of multiunit amines for more efficient solid-state amino-MOF adsorbents.

MATERIALS AND METHODS

Materials Synthesis. 2,5-Dihydroxyterephtlaic acid (H_4-DOBDC, 98%), magnesium nitrate hexahydrate ($(Mg(NO_3)_2{\cdot}6H_2O$, ACS reagent 99%), anhydrous toluene (99.8%), and tetraethylenepentamine (technical grade) were purchased from Sigma-Aldrich without

DOI: 10.1021/acsami.7b02471
ACS Appl. Mater. Interfaces 2017, 9, 11299−11306

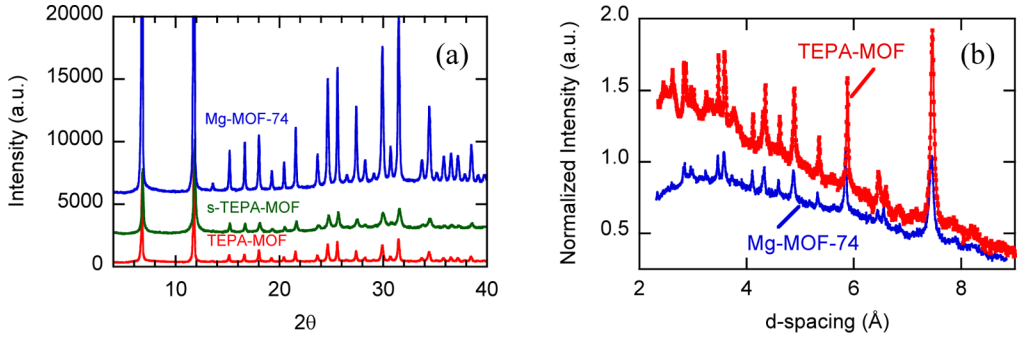

Figure 1. (a) XRD patterns for pristine and TEPA-functionalized MOFs. (b) Neutron powder diffraction patterns for as-synthesized and TEPA-functionalized Mg-MOF. The sloping baseline is due to the presence of hydrogen.

further purification. Mg-MOF-74 was synthesized according to literature methods.[12,13,42]

Series 1. The linker 2,5-dihydroxy-therepthalic acid (DHTA, 0.337 g, 1.65 mmol) and metal source ($Mg(NO_3)_2{\cdot}6H_2O$ (1.4 g, 5.46 mmol)) were dissolved in 153 mL of a DMF, ethanol, and water mixture ((15:1:1 v/v/v). The solution was split into 15 scintillation vials (20 mL each), capped, and kept at 125 °C for 26 h. Dark yellow material formed on the walls of the vials, which was collected, and the solvent was exchanged with methanol every 8 h, for a total of 4−5 washes. The paste was then dried at 80 °C in a vacuum oven. The yield of the reaction was close to 100% based on the weight of the organic linker. The resulting powder was analyzed by using powder XRD, XPS, and FTIR. BET surface area of the Mg-MOF-74 was measured to be ∼800 m^2/g after activation at 150 °C for 4 h.

Series 2. Linker DHTA (0.112 g, 0.57 mmol) and $Mg(NO_3)_2{\cdot}6H_2O$ (0.475 g, 1.85 g) were dissolved in a mixture of DMF (45 mL), ethanol (4 mL), and water (3 mL). The solution was placed in a Teflon-lined autoclave and kept at 125 °C for 21 h. The resulting solids were washed with methanol for 8 h (5 times) and then dried under vacuum. The resulting MOF was activated at 250 °C under nitrogen atmosphere for 6 h. BET surface area of the series 2 materials was measured to be 1628 m^2/g (Figure S5). Both series 1 and 2 of the MOF material were subjected to the CO_2 and water vapor sorption studies.

For the amine functionalization, the series 2 MOF (50 mg) and TEPA (1.15 g) were dissolved in a glass reaction vessel with 20 mL of toluene, and the mixture was refluxed under argon flow for 24 h. The resulting material, termed s-TEPA-MOF due to the saturation of the surface sites, was filtered off and washed with copious amounts of toluene and methanol. After the initial functionalization and washing, subsequent washing and soaking in toluene and methanol did not remove the amine molecules from the MOFs (by XPS surface analysis), demonstrating strong chemical binding of TEPA to the MOF. An analogous procedure was carried out with 0.0115 g of TEPA and 50 mg of Mg-MOF-74, and the resulting material with lower degree of functionalization is termed TEPA-MOF. Control batch Mg-MOF-74 was activated at 250 °C under vacuum. For the TEPA-modified MOF, 150 °C was used as the activation temperature, due to potential degradation of the amines at $T > 150$ °C.

Material Characterization. X-ray powder diffraction (XRD) was carried out using the Bruker PanAlytical instrument, with an X'celerator high-speed detector, and 0.02 soller slits, with a Ni β filter and Cu Kα beam. Programmable divergence slits were applied for a constant length of incidence on the samples (4 mm). BET surface area was obtained using a Micromeritics ASAP 2020 with N_2 adsorption at 77 K. The Physical Electronics Versaproble II X-ray photoelectron spectrometer (XPS) was used for the analysis of the surface of the electrodes. The analysis was performed at ultrahigh vacuum (1×10^{-8} bar) with an argon-gun neutralizer. The survey scans were performed with 10 cycles from 1400 to 50 eV at 200 kV with a pass energy of 80 eV and a step size of 0.5 eV. The high-resolution scans were performed at 100 kV, a pass energy of 11 eV, and 0.05 eV resolution with 30 cycles for iron and 8 cycles for the remaining elements. The scans were exported using CASA XPS commercial software (MIT license), and peak fitting was performed using XPS Peak Fit freeware. The surface morphology of the electrodes was characterized by a FEG-XL-30 field-emission SEM at 20 kV using a beam size of 3 and high-vacuum conditions, and a ZEISS Merlin High-Resolution SEM at 5 kV-20 kV. Energy dispersive X-ray spectroscopy (EDX) was performed using the TEAM software to map the elements at 50 μs dwell time, 512 × 400 resolution, and 15 kV. Neutron diffraction was performed on the TEPA-MOF as well as Mg-MOF-74 at the Powgen Powder Diffractometer located at the Spallation Neutron Source (SNS), Oak Ridge National Laboratory. Center wavelengths of 2.665 and 4.797 Å were used to collect data within the d-spacing range 1−10 Å. Due to the presence of hydrogen, a relatively large background was observed in the neutron data, especially at the shorter d-spacings. Good quality data were only collected for the longer d-spacings at 20 and 300 K using an autochanger fitted with a standard close cycle refrigerator (CCR). Thermogravimetric analysis (TGA) and simultaneous differential scanning calorimetry (DSC) were conducted using a Q600 TGA/DSC instrument (TA Instruments, Inc.). Samples were subjected to heating scans (20 °C/min) in a temperature ramp mode.

Gravimetric Dynamic Vapor Sorption (DVS Vacuum). The CO_2 and H_2O sorption and CO_2/H_2O competitive sorption isotherms were measured using a dynamic gravimetric vapor sorption analyzer, DVS vacuum (Surface Measurement Systems Ltd., London, UK). Data were recorded in a dynamic mode, whereby DVS vacuum can control and measure sorbate entry and exit flows simultaneously while recording change in the mass. The uptake and loss of sorbate were measured gravimetrically on an Ultrasensitive stage2 microbalance (Surface Measurement Systems Ltd., London, UK) which has sensitivity of 0.1 μg and peak-to-peak noise less than 0.3 μg. The water vapor generation/delivery system and sample chamber were maintained at constant temperature (≤0.1 °C) in the temperature-controlled enclosure working at a temperature ranging between 20 and 70 °C. The pressure was measured by three transducers (MicroPirani, 10 and 1000 Torr absolute pressure transducers). Fully automated DVS vacuum is controlled by Vacuum Control Software that allows users to program method parameters such as sorption experimental temperature (20 to 400 °C), multiple *in situ* degassing temperature steps, relative pressure steps, and flow rates. MOF samples were *in situ* degassed under high vacuum (1×10^{-5} Torr) and temperature of 150 °C for 4 h and then cooled down to sorption temperature before immediate CO_2 or H_2O adsorption. The adsorption/desorption cycles showing H_2O and H_2O/CO_2 sorption kinetics were performed at 25 °C at a saturation vapor pressure of P_0 of 23.8 Torr, and relative pressures were varied from 1 to 90% of P/P_0. CO_2 adsorption/desorption measurements were performed at pressures from 0 to 760 Torr with small pressure steps. The mass equilibration rates of MOFs at each relative pressure step were controlled on the basis of the mass equilibrium criterion, dm/dt (%/min), and time (min). Differential CO_2 adsorption was also performed on TEPA-MOF and MOF-74 using a Quantachrome AS iQ with a temperature-controller assembly for adsorption.

DOI: 10.1021/acsami.7b02471
ACS Appl. Mater. Interfaces 2017, 9, 11299−11306

Table 1. Lattice Parameters from Rietveld Refinement for Mg-MOF-74 and Amine-Functionalized MOF

structure	a	c	V	Rwp (%)	χ^2
Mg-MOF 74 (300 K)	25.8151(13)	6.8980(6)	3981.1(4)	1.81	7.8
TEPA-MOF (300 K)	25.7544(18)	6.8405(9)	3929.4(7)	1.17	5.0
TEPA-MOF (20 K)	25.7887(22)	6.8685(10)	3955.9(7)	1.08	4.2

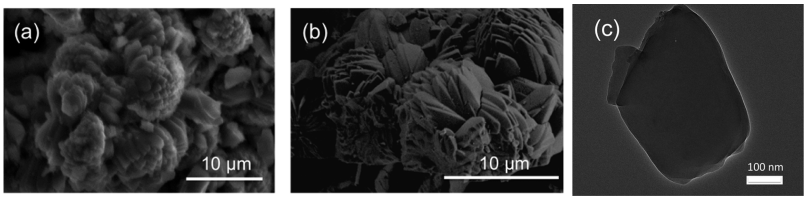

Figure 2. High-resolution FE-SEM on (a) Mg-MOF-74 and (b) TEPA-MOF. (c) The single crystallite of dispersed MOF after functionalization.

RESULTS AND DISCUSSION

Structural Characterization. Powder XRD patterns are shown in Figure 1a for unmodified but activated series 2 Mg-MOF-74 and TEPA-modified Mg-MOF-74. The XRD patterns (ratio of intensities and position) for the two different functionalized MOFs are essentially no different from those of the native Mg-MOF-74, indicating that the MOF structure remained unaltered during the activation and modification processes. The Mg-MOF-74 structure is composed of trigonal cells with crystallographic indexes a = 26.02 Å and c = 6.721 Å, and of hexahedral cylindrical pores that strongly bind CO_2.[13] Rietveld refinement of our neutron diffraction data shown in Figure 1b indicates that there is a slight cell contraction when the as-synthesized Mg-MOF-74 is functionalized to produce TEPA-MOF. The lattice parameter decreases by 0.3% in the a-coordinate and 0.8% in the c-coordinate, corresponding to a volume decrease of 1.3%, as shown in Table 1. The slight difference in relative peak intensities, with the same spacing, indicates a distinct effect of incorporated amines on the bulk crystal structure. Since no additional diffraction peaks were present in either the Mg-MOF-74 or the TEPA-MOF spectra, it can be concluded that the amines were disordered within the structures. This is further supported by the fact that the unit-cell symmetry group is preserved (hexagonal), which is a strong argument against the formation of an ordered supercell with amines oriented along the pore walls. Interestingly, the TEPA-MOF undergoes slight cell contraction between 300 and 20 K (see Table 1), which may indicate its potential as a negative thermal expansion (NTE) material.[43,44] The SEM images of MOF particles in Figure 2a,b show that they exist as flower-like aggregates of ∼3−8 μm crystals and that they maintain their morphology after functionalization; this observation is corroborated by TEM images on the dispersed MOF crystals in methanol of nanocrystallites of 500−800 nm (Figure 2c). The characteristic size and textural properties of the MOF particles are similar to those prepared by solvothermal synthesis.[18]

The distribution of TEPA within the porous structure of the modified MOF is of interest, as it may affect its CO_2 sorbent performance. The Mg-MOF-74 cell is composed of 18 Mg, 72 C, 18 H, and 54 O atoms, with each Mg coordinated to 4 oxygens, and the Mg-MOF-74 XPS survey spectra indicate that the compositions at the surface and within the bulk of the particles are comparable (Table 2). The XPS survey (Figure 3a) shows an increase in surface amino groups due to the increase in the nitrogen N 1s peak, which is absent from the native Mg-MOF-74. The high-resolution Mg 2p3 scans, shown in Figure 3b, indicate an approximately 1.5 eV lower binding energy shift for the saturated MOF (∼47 eV for s-TEPA-MOF vs 48.5 eV for Mg-MOF-74). This shift is due to the different environment for the magnesium on the surface of the functionalized TEPA-MOF from that on the unmodified Mg-MOF-74, an indication of possible amine−Mg complexation. The XPS shift to lower binding energies is consistent with amine−metal complexation by electron donation, as the Mg-center becomes more electronegative after accepting the electron pair from the primary amine donor.[45,46]

Table 2. Surface versus Bulk Characterization of Amine-Functionalized MOF Materials

	s-TEPA-MOF	TEPA-MOF	Mg-MOF-74
Composition by XPS (at %)			
N	19.38	10.77	
Mg	4.52	7.15	9.33
O	21.7	54.03	54.4
C	54.03	28.5	36.2
Composition by Elemental Analysis (at %)			
N	1	0.7	theoretical
Mg	11	10	12.5
O	50	54	37.5
C	38	48	50
Amine Surface-to-Bulk Ratio			
	0.85	0.3	0

The penetration depth in XPS experiments is 8−10 nm in most samples, corresponding to approximately 10 unit cells, while the characteristic size of the MOF particles is typically 500 nm to 1 μm (Figure 1 SEM/TEM images). The surface composition of the MOF particles revealed by XPS was compared to total elemental composition, obtained from ICP measurements made by the consumption and dissolution of the entire particle. The ratio of N to Mg derived from XPS is ca. 5 for the saturated s-TEPA-MOF, which indicates that each surface Mg-site is bound to one TEPA molecule (0.85 ratio of TEPA to Mg-center). On the other hand, TEPA-MOF with a lower degree of functionalization yields a surface TEPA to Mg ratio of 0.3, which is roughly 2 TEPA per 5 Mg-centers. This high amine loading is restricted primarily to the top layers of the MOF, as the elemental analysis of the bulk TEPA-MOF indicates that the total nitrogen and Mg contents of the particles are 0.7 and 11 wt %, respectively (Table 2). The much higher amine content on the surface relative to that in the bulk indicates that the concentration of TEPA is highest within the

DOI: 10.1021/acsami.7b02471
ACS Appl. Mater. Interfaces 2017, 9, 11299−11306

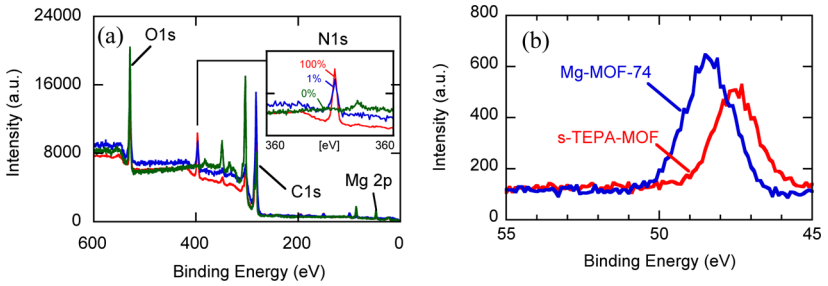

Figure 3. (a) Survey XPS scans for various modified MOFs (series 1 and 2) illustrating functionalization. (b) High-resolution Mg 2p3 scan between saturated s-TEPA-MOF and original Mg-MOF-74.

unit-cell layers of the MOF in the proximity of the particle surface. Some incorporation of the TEPA molecules in the bulk of the particle can still be anticipated, however, and the presence of amine molecules throughout the crystals would be sufficient to cause the changes in lattice parameters observed by neutron diffraction (Table 1).

CO_2 Sorption. The distribution of amines on and within the functionalized Mg-MOF-74 particles strongly affected the extent of CO_2 adsorption observed in dynamic vapor sorption (DVS) and static volumetric sorption measurements. Despite its higher surface amine loading, the amine-saturated s-TEPA-MOF species exhibited a significantly lower CO_2 uptake capacity than did TEPA-MOF, attributed to a steric hindrance to gas transport offered by the dense TEPA film on the surface of the saturated MOF. The TEPA-MOF species also showed a marked 11% wt increase in uptake capacity relative to that of the native MOF based on total adsorbent basis (TEPA + MOF), but if we take the native MOF as the mass basis, the increase is close to 15% (26.9 wt % TEPA-MOF vs 23.4 wt % Mg-MOF-74). This increase in CO_2 capacity with a low degree of functionalization with TEPA can be attributed both to an increase in extra available binding sites from the amines, which provides a higher density of active site/mass than the metal centers, and to the accessibility of the bulk unsaturated Mg-sites within the MOFs; when the surface is saturated with an impermeable layer of amines, accessibility to the Mg-sites deep within the crystals is restricted. Of practical importance, the DVS adsorption/desorption isotherms in Figure 4 exhibited no discernible pressure hysteresis, and with a desorption temperature of 120 °C all of the CO_2 adsorbed at 1 atm partial pressure was released. We can conclude that irreversible carbamate formation or other reactions of CO_2 with TEPA did not take place over the temperature range studied.

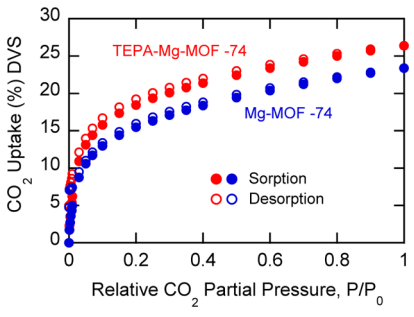

Figure 4. Mg-MOF-74 (series 1) and corresponding TEPA-MOF CO_2 adsorption/desorption weight uptake (%) based on total adsorbent mass (TEPA + MOF), in the pressure range from 0 to 760 Torr and 25 °C.

The BET CO_2 sorption and desorption measurements using a static volumetric method (Figure 5) indicated a significantly

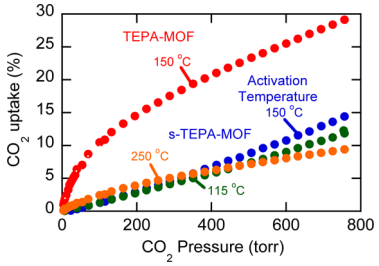

Figure 5. Comparison of CO_2 adsorption isotherms at 25 °C of functionalized TEPA-MOF with s-TEPA-MOF activated at varying temperatures using static volumetric CO_2 sorption method. Blended batches of Mg-MOF-74 (series 1 and 2) were utilized as a parent material for the amine functionalization.

higher CO_2 adsorption capacity for TEPA-MOF than for its saturated s-TEPA-MOF counterpart. Indeed, the s-TEPA-MOF species with activation temperatures ranging from 110 to 250 °C showed a much lower CO_2 uptake level, with a less than 10 wt % CO_2 adsorption capacity at 25 °C, than did either TEPA-MOF or the parent Mg-MOF-74. The choice of 150 °C under vacuum as the activation temperature for the amine-functionalized systems was found to be optimal for carbon dioxide adsorption (higher temperatures lead to the amine degradation), as opposed to the unmodified Mg-MOF-74, wherein activation at 250 °C preserves capacity.[47] Exposure of the amine-loaded MOF to 250 °C in nitrogen atmosphere resulted in the significant reduction of the modified MOF's ability to sorb either water vapors or CO_2, or both, from their mixtures (Figures S6 and S7). Thermogravimetric analysis demonstrated that approximately half of the TEPA added to the parent MOF that had been activated at 250 °C decomposed and was lost after the subsequent exposure of the TEPA-MOF at 250 °C in a 20 °C/min heating ramp (Figure S8). It is safe to assume that the elimination of the amine from the TEPA-MOF was even more extensive upon degassing of the TEPA-MOF at 250 °C for several hours in the sorption experiments. These results explain the diminished sorption capacity of thus activated TEPA-MOF and justify the MOF activation at lower temperatures.

The decreased adsorption by s-TEPA-MOF relative to that of TEPA-MOF can be attributed to the excess functionalization on the surface, which forms a film to prevent CO_2 from accessing the bulk Mg-sites. TEPA-MOF, with a lower degree of surface TEPA functionalization, allows both the bulk Mg-sites and the additional surface TEPA to be accessed, so that

DOI: 10.1021/acsami.7b02471
ACS Appl. Mater. Interfaces 2017, 9, 11299−11306

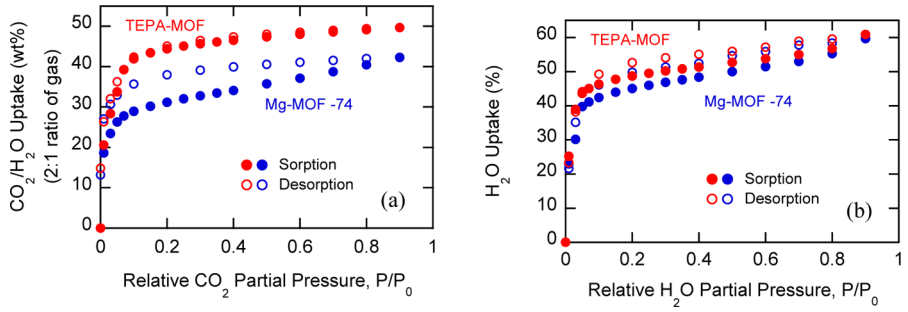

Figure 6. (a) 2/1 CO_2/H_2O adsorption/desorption equilibria at 25 °C for Mg-MOF-74 and TEPA-MOF (P_0 = 23 Torr for water) and (b) pure H_2O vapor sorption up to 23 Torr.

the CO_2 capacity is increased. This effect has also been observed in the impregnation of polyamines into mesoporous silica, in which the chemisorption properties of the material were improved but the pore access was impeded by the larger amine molecules.[38] Polyamines with alkyl chains of over 13 carbon atoms tended to significantly decrease the gas adsorption capacities of other porous materials.[41,48,49] Furthermore, even with the magnesium-based MOFs, the structure of the amines can impact the amine−CO_2 binding stoichiometry, which depends on the arrangement of the amines with respect to the coordinatively unsaturated metal sites of the MOF.[50]

Water Stability. Functionalization of the Mg-MOF-74 by TEPA was also shown to have beneficial effects on the MOF stability in humid environments. The DVS studies were conducted with a CO_2/H_2O ratio of 2:1 (similar to that of coal-fired power plant flue gas streams), with H_2O under controlled pressure (P/P_0), up to the saturation vapor pressure of water at 25 °C (P_0 = 23 Torr). In these experiments, the overall sorption capacity of the functionalized MOF was superior to that of the Mg-MOF-74 material (Figure 6a). Water affected the Mg-MOF-74 capacity much more significantly than the capacity of the functionalized MOF. The adsorption of pure water vapor by both MOFs was approximately the same under a wide range of partial pressures at 25 °C (see Figure 6b), with very similar uptake values for the functionalized and parent MOFs at saturation (~59 wt % H_2O at P_0), with a distinct hysteresis loop indicating strong chemisorption of H_2O onto the coordinatively unsaturated metal centers. The high uptake of ~59 wt % at H_2O saturation corresponds very closely to previously reported values in the literature for vapor sorption by both solvothermally and sonochemically synthesized Mg-MOF-74 particles.[18] However, in the case of the 2:1 CO_2/H_2O, which reflects flue-gas compositions more closely, there was a distinct increased uptake by TEPA-MOF relative to that by the parent material. In addition, a significant hysteresis in the CO_2/water adsorption/desorption cycle was observed for Mg-MOF-74 after desorption, indicating that H_2O binding occurred even at the lower humidity. With the TEPA-functionalized MOF, however, the uptake was fully reversible over the full pressure range, indicating that the surface H_2O and bulk CO_2 adsorbed can be easily captured and released by pressure swing cycling, and that the TEPA-MOF is a more robust material for carbon capture under wet conditions. The higher uptake of CO_2 by TEPA-MOF than by Mg-MOF-74 can be attributed to chemical protection of the MOF structure by the TEPA ligand, as seen previously with ethylene diamine coverage.[35]

CONCLUSIONS

In the schematic shown in Figure 7, we summarize our findings that the CO_2 adsorption under both dry and humid conditions

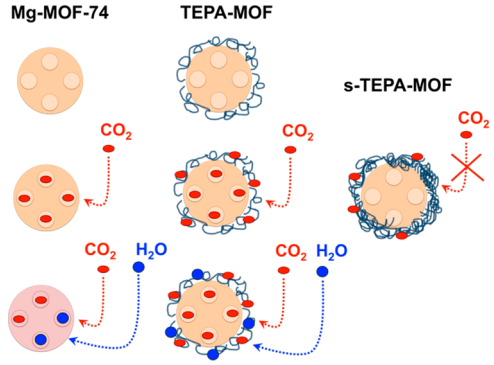

Figure 7. TEPA-functionalization (in blue) of Mg-MOF-74 and its effect on CO_2 (in red) adsorption depending on degree of saturation (s-TEPA being saturated particle). The native Mg-MOF allows both H_2O and CO_2 to enter and thus damage the crystal structure, whereas in the TEPA case the amine layer protects the bulk MOF against H_2O entry.

is affected strongly by the degree of functionalization of the parent Mg-MOF-74 particles with TEPA. Indeed, with partial amine functionalization, we obtain a CO_2 adsorption capacity beyond the already high values observed for the parent unmodified MOF. The TEPA-MOF shows q = 26.9 wt % versus 23.4 wt % (by DVS) CO_2 adsorption uptake for MOF-74 at 25 °C, based on the amine-free MOF weight, which indicates an increase over parent MOF capacity of close to 15%, with a static volumetric adsorption of up to 30 wt % at 1 bar. The XPS and neutron diffraction studies indicated that the amines are distributed nonhomogeneously through the MOF particle, with a higher degree of impregnation on the top layer pores and surface than in the inner bulk cavities, as seen by the higher N content observed by XPS than by ICP on the dissolved particles. At the same time, TEPA impregnation causes slight changes in the crystal structure resolved by neutron diffraction, consistent with the elemental analysis that indicated an incorporation of the amines within the bulk of the crystal, far from its surface. This structural characterization shed light on the role played by the amines used to functionalize Mg-MOF-74 in achieving higher CO_2 capacity. TEPA, in contrast to diamines, increases CO_2 adsorption based on stoichiometric site binding onto the MOFs not only in the dilute pressure range previously shown (<0.05 bar), but also in the moderate pressure range (0.1−1 bar). Furthermore, under humid

DOI: 10.1021/acsami.7b02471
ACS Appl. Mater. Interfaces 2017, 9, 11299−11306

conditions similar to those found in power plant flue gases, TEPA-MOF seems to protect the adsorbent against water adsorption and preserves significant CO_2 adsorption capacity. CO_2 adsorption seems to be preserved significantly for the TEPA-MOF over Mg-MOF-74 (~50 wt % uptake for TEPA-MOF vs ~39 wt % uptake for Mg-MOF-74 under 2:1 CO_2:H_2O conditions), and as such we have shown that TEPA-functionalized MOFs can provide stable Mg-based MOFs for flue-gas applications.

In summary, our work has shown the distinct advantages of using multiunit amines over diamines in the functionalization of Mg-MOF-74 particles, and we expect that further molecular optimization such as that of amine size and chemical nature coupled with MOFs of complementary structural characteristics (e.g., sufficiently large pore sizes and number of anchoring groups) will lead to higher density of the more accessible binding sites, and that progressive design of these molecular systems will bring the field deployment of the solid-state CO_2 adsorbents closer to practice.

■ ASSOCIATED CONTENT

Supporting Information

The Supporting Information is available free of charge on the ACS Publications website at DOI: 10.1021/acsami.7b02471.

Rietveld refinement of Mg-MOF-74 and TEPA-MOF XRD data, TEM images, BET adsorption isotherms, CO_2 and water vapor adsorption−desorption isotherms, and thermogravimetric analysis of the Mg-MOF-74 and its TEPA-modified product (PDF)

■ AUTHOR INFORMATION

Corresponding Author

*E-mail: tahatton@mit.edu.

Notes

The authors declare no competing financial interest.

■ ACKNOWLEDGMENTS

We thank Franziska Kazenwadel and Ryan Friederich for help with the synthesis of Mg-MOF-74, Scott Speakman for support with the XRD measurements, and Charles Settens for helpful discussions on X-ray diffraction.

■ REFERENCES

(1) Cox, P. M.; Betts, R. A.; Jones, C. D.; Spall, S. A.; Totterdell, I. J. Acceleration of Global Warming due to Carbon-cycle Feedbacks in a Coupled Climate Model. *Nature* **2000**, *408*, 184−187.

(2) Hughes, T. P.; Baird, A. H.; Bellwood, D. R.; Card, M.; Connolly, S. R.; Folke, C.; Grosberg, R.; Hoegh-Guldberg, O.; Jackson, J. B. C.; Kleypas, J.; Lough, J. M.; Marshall, P.; Nystrom, M.; Palumbi, S. R.; Pandolfi, J. M.; Rosen, B.; Roughgarden, J. Climate Change, Human Impacts, and the Resilience of Coral Reefs. *Science* **2003**, *301*, 929−933.

(3) Hoegh-Guldberg, O.; Mumby, P. J.; Hooten, A. J.; Steneck, R. S.; Greenfield, P.; Gomez, E.; Harvell, C. D.; Sale, P. F.; Edwards, A. J.; Caldeira, K.; Knowlton, N.; Eakin, C. M.; Iglesias-Prieto, R.; Muthiga, N.; Bradbury, R. H.; Dubi, A.; Hatziolos, M. E. Coral Reefs under Rapid Climate Change and Ocean Acidification. *Science* **2007**, *318*, 1737−1742.

(4) D'Alessandro, D. M.; Smit, B.; Long, J. R. Carbon Dioxide Capture: Prospects for New Materials. *Angew. Chem., Int. Ed.* **2010**, *49*, 6058−6082.

(5) Wang, Q.; Luo, J.; Zhong, Z.; Borgna, A. CO2 Capture by Solid Adsorbents and their Applications: Current Status and New Trends. *Energy Environ. Sci.* **2011**, *4*, 42−55.

(6) Valenzano, L.; Civalleri, B.; Chavan, S.; Palomino, G. T.; Arean, C. O.; Bordiga, S. Computational and Experimental Studies on the Adsorption of CO, N2, and CO2 on Mg-MOF-74. *J. Phys. Chem. C* **2010**, *114*, 11185−11191.

(7) Seoane, B.; Coronas, J.; Gascon, I.; Benavides, M. E.; Karvan, O.; Caro, J.; Kapteijn, F.; Gascon, J. Metal-Organic Framework Based Mixed Matrix Membranes: a Solution for Highly Efficient CO2 Capture? *Chem. Soc. Rev.* **2015**, *44*, 2421−2454.

(8) Ferey, G. Hybrid Porous Solids: Past, Present, Future. *Chem. Soc. Rev.* **2008**, *37*, 191−214.

(9) Li, J. R.; Kuppler, R. J.; Zhou, H. C. Selective Gas Adsorption and Separation in Metal-Organic Frameworks. *Chem. Soc. Rev.* **2009**, *38*, 1477−1504.

(10) Murray, L. J.; Dinca, M.; Long, J. R. Hydrogen Storage in Metal-Organic Frameworks. *Chem. Soc. Rev.* **2009**, *38*, 1294−1314.

(11) Li, H.; Eddaoudi, M.; O'Keeffe, M.; Yaghi, O. M. Design and synthesis of an exceptionally stable and highly porous metal-organic framework. *Nature* **1999**, *402*, 276−279.

(12) Britt, D.; Furukawa, H.; Wang, B.; Glover, T. G.; Yaghi, O. M. Highly Efficient Separation of Carbon dioxide by a Metal-organic Framework Replete with Open Metal Sites. *Proc. Natl. Acad. Sci. U. S. A.* **2009**, *106*, 20637−20640.

(13) Caskey, S. R.; Wong-Foy, A. G.; Matzger, A. J. Dramatic Tuning of Carbon Dioxide Uptake via Metal Substitution in a Coordination Polymer with Cylindrical Pores. *J. Am. Chem. Soc.* **2008**, *130*, 10870−10871.

(14) Yazaydin, A. O.; Snurr, R. Q.; Park, T.-H.; Koh, K.; Liu, J.; LeVan, M. D.; Benin, A. I.; Jakubczak, P.; Lanuza, M.; Galloway, D. B.; Low, J. J.; Willis, R. R. Screening of Metal-Organic Frameworks for Carbon Dioxide Capture from Flue Gas Using a Combined Experimental and Modeling Approach. *J. Am. Chem. Soc.* **2009**, *131*, 18198−18199.

(15) Pera-Titus, M. Porous Inorganic Membranes for CO2 Capture: Present and Prospects. *Chem. Rev.* **2014**, *114*, 1413−1492.

(16) Harada, T.; Hatton, T. A. Colloidal Nanoclusters of MgO Coated with Alkali Metal Nitrates/Nitrites for Rapid, High Capacity CO2 Capture at Moderate Temperature. *Chem. Mater.* **2015**, *27*, 8153−8161.

(17) Harada, T.; Simeon, F.; Hamad, E. Z.; Hatton, T. A. Alkali Metal Nitrate-Promoted High-Capacity MgO Adsorbents for Regenerable CO2 Capture at Moderate Temperatures. *Chem. Mater.* **2015**, *27*, 1943−1949.

(18) Yang, D. A.; Cho, H. Y.; Kim, J.; Yang, S. T.; Ahn, W. S. CO2 Capture and Conversion Using Mg-MOF-74 Prepared by a Sonochemical Method. *Energy Environ. Sci.* **2012**, *5*, 6465−6473.

(19) Queen, W. L.; Brown, C. M.; Britt, D. K.; Zajdel, P.; Hudson, M. R.; Yaghi, O. M. Site-Specific CO 2 Adsorption and Zero Thermal Expansion in an Anisotropic Pore Network. *J. Phys. Chem. C* **2011**, *115*, 24915−24919.

(20) Juan-Alcaniz, J.; Gascon, J.; Kapteijn, F. Metal-organic frameworks as scaffolds for the encapsulation of active species: state of the art and future perspectives. *J. Mater. Chem.* **2012**, *22*, 10102−10118.

(21) Burrows, A. D.; Frost, C. G.; Mahon, M. F.; Richardson, C. Post-Synthetic Modification of Tagged Metal-Organic Frameworks. *Angew. Chem., Int. Ed.* **2008**, *47*, 8482−8486.

(22) Sculley, J.; Yuan, D. Q.; Zhou, H. C. The Current Status of Hydrogen Storage in Metal-Organic Frameworks-Updated. *Energy Environ. Sci.* **2011**, *4*, 2721−2735.

(23) Valtchev, V.; Majano, G.; Mintova, S.; Perez-Ramirez, J. Tailored Crystalline Microporous Materials by Post-Synthesis Modification. *Chem. Soc. Rev.* **2013**, *42*, 263−290.

(24) Lalonde, M.; Bury, W.; Karagiaridi, O.; Brown, Z.; Hupp, J. T.; Farha, O. K. Transmetalation: Routes to Metal Exchange Within Metal-Organic Frameworks. *J. Mater. Chem. A* **2013**, *1*, 5453−5468.

(25) Lee, W. R.; Hwang, S. Y.; Ryu, D. W.; Lim, K. S.; Han, S. S.; Moon, D.; Choi, J.; Hong, C. S. Diamine-Functionalized Metal-Organic Framework: Exceptionally High CO2 Capacities from

DOI: 10.1021/acsami.7b02471
ACS Appl. Mater. Interfaces 2017, 9, 11299−11306

Ambient Air and Flue Gas, Ultrafast CO2 Uptake Rate, and Adsorption Mechanism. *Energy Environ. Sci.* **2014**, *7*, 744−751.
(26) Lee, W. R.; Jo, H.; Yang, L. M.; Lee, H.; Ryu, D. W.; Lim, K. S.; Song, J. H.; Min, D. Y.; Han, S. S.; Seo, J. G.; Park, Y. K.; Moon, D.; Hong, C. S. Exceptional CO2 Working Capacity in a Heterodiamine-grafted Metal-Organic Framework. *Chem. Sci.* **2015**, *6*, 3697−3705.
(27) McDonald, T. M.; Lee, W. R.; Mason, J. a.; Wiers, B. M.; Hong, C. S.; Long, J. R. Capture of Carbon Dioxide from Air and Flue gas in the Alkylamine-Appended Metal-Organic Framework mmen-Mg2-(dobpdc). *J. Am. Chem. Soc.* **2012**, *134*, 7056−7065.
(28) Liao, P. Q.; Chen, X. W.; Liu, S. Y.; Li, X. Y.; Xu, Y. T.; Tang, M. N.; Rui, Z. B.; Ji, H. B.; Zhang, J. P.; Chen, X. M. Putting an Ultrahigh Concentration of Amine Groups into a Metal-organic Framework for CO2 Capture at Low Pressures. *Chem. Sci.* **2016**, *7*, 6528−6533.
(29) McDonald, T. M.; Mason, J. A.; Kong, X. Q.; Bloch, E. D.; Gygi, D.; Dani, A.; Crocella, V.; Giordanino, F.; Odoh, S. O.; Drisdell, W. S.; Vlaisavljevich, B.; Dzubak, A. L.; Poloni, R.; Schnell, S. K.; Planas, N.; Lee, K.; Pascal, T.; Wan, L. W. F.; Prendergast, D.; Neaton, J. B.; Smit, B.; Kortright, J. B.; Gagliardi, L.; Bordiga, S.; Reimer, J. A.; Long, J. R. Cooperative Insertion of CO2 in Diamine-Appended Metal-Organic Frameworks. *Nature* **2015**, *519*, 303−308.
(30) Bromberg, L.; Su, X.; Hatton, T. A. Heteropolyacid-Functionalized Aluminum 2-Aminoterephthalate Metal-Organic Frameworks As Reactive Aldehyde Sorbents and Catalysts. *ACS Appl. Mater. Interfaces* **2013**, *5*, 5468−5477.
(31) Bromberg, L.; Su, X.; Hatton, T. A. Aldehyde Self-Condensation Catalysis by Aluminum Aminoterephthalate Metal-Organic Frameworks Modified with Aluminum Isopropoxide. *Chem. Mater.* **2013**, *25*, 1636−1642.
(32) Bromberg, L.; Su, X.; Hatton, T. A. Functional Networks of Organic and Coordination Polymers: Catalysis of Fructose Conversion. *Chem. Mater.* **2014**, *26*, 6257−6264.
(33) Kim, S. N.; Yang, S. T.; Kim, J.; Park, J. E.; Ahn, W. S. Post-synthesis Functionalization of MIL-101 using diDethylenetriamine: a Study on Adsorption and Catalysis. *CrystEngComm* **2012**, *14*, 4142−4147.
(34) Choi, S.; Watanabe, T.; Bae, T.-h.; Sholl, D. S.; Jones, C. W. Modification of the Mg/DOBDC MOF with Amines to Enhance CO2 Adsorption from Ultradilute Gases. *J. Phys. Chem. Lett.* **2012**, *3*, 1136−1141.
(35) Andirova, D.; Lei, Y.; Zhao, X. D.; Choi, S. H. Functionalization of Metal-Organic Frameworks for Enhanced Stability under Humid Carbon Dioxide Capture Conditions. *ChemSusChem* **2015**, *8*, 3405−3409.
(36) Demessence, A.; D'Alessandro, D. M.; Foo, M. L.; Long, J. R. Strong CO2 Binding in a Water-Stable, Triazolate-Bridged Metal-Organic Framework Functionalized with Ethylenediamine. *J. Am. Chem. Soc.* **2009**, *131*, 8784−8786.
(37) Vilarrasa-Garcia, E.; Moya, E. M. O.; Cecilia, J. A.; Cavalcante, C. L., Jr.; Jimenez-Jimenez, J.; Azevedo, D. C. S.; Rodriguez-Castellon, E. CO2 Adsorption on Amine Modified Mesoporous Silicas: Effect of the Progressive Disorder of the Honeycomb Arrangement. *Microporous Mesoporous Mater.* **2015**, *209*, 172−183.
(38) Xu, X. C.; Song, C. S.; Wincek, R. T.; Andresen, J. A.; Miller, B. G.; Scaroni, A. W. Separation of CO2 from Power Plant Flue Gas using a Novel CO2 "Molecular Basket" Adsorbent. *Abstr. Pap. Am. Chem. Soc.* **2003**, *225*, U854−U855.
(39) Zevenhoven, R.; Kilpinen, P. *Control of Pollutants in Flue Gases and Fuel Gases*; Helisinki University of Technology: Turku, Finland, 2001.
(40) Han, S. S.; Choi, S.-H.; van Duin, A. C. T. Molecular Dynamics Simulations of Stability of Metal−Organic Frameworks against H2O using the ReaxFF Reactive Force Field. *Chem. Commun.* **2010**, *46*, 5713−5715.
(41) Gibson, J. A. A.; Gromov, A. V.; Brandani, S.; Campbell, E. E. B. The Effect of Pore Structure on the CO2 Adsorption Efficiency of Polyamine Impregnated Porous Carbons. *Microporous Mesoporous Mater.* **2015**, *208*, 129−139.
(42) Glover, T. G.; Peterson, G. W.; Schindler, B. J.; Britt, D.; Yaghi, O. MOF-74 Building Unit has a Direct Impact on Toxic Gas Adsorption. *Chem. Eng. Sci.* **2011**, *66*, 163−170.
(43) Margadonna, S.; Prassides, K.; Fitch, A. N. Zero Thermal Expansion in a Prussian blue Analogue. *J. Am. Chem. Soc.* **2004**, *126*, 15390−15391.
(44) Phillips, A. E.; Halder, G. J.; Chapman, K. W.; Goodwin, A. L.; Kepert, C. J. Zero Thermal Expansion in a Flexible, Stable Framework: Tetramethylammonium Copper(I) Zinc(II) Cyanide. *J. Am. Chem. Soc.* **2010**, *132*, 10−11.
(45) Akolekar, D. B.; Kaliaguine, S. MAPO-43 Molecular-sieve - Synthesis, Characterization and Thermal Stability. *Microporous Mater.* **1994**, *2*, 137−144.
(46) Moulder, J. F.; Stickle, W. F.; Sobol, P. E.; Bomben, K. D. *Handbook of X-ray Photoelectron Spectroscopy*; Physical Electronics, Inc: Eden Prairie, MN, 1992.
(47) Mason, J. A.; Sumida, K.; Herm, Z. R.; Krishna, R.; Long, J. R. Evaluating Metal-Organic Frameworks for Post-Combustion Carbon Dioxide Capture via Temperature Swing Adsorption. *Energy Environ. Sci.* **2011**, *4*, 3030−3040.
(48) Lee, D. Y.; Zhang, C. Y.; Gao, H. F. Amine-Functionalized Porous Polymer Network for Highly Selective Absorption of CO2 Over N2. *Macromol. Chem. Phys.* **2015**, *216*, 489−494.
(49) Zhang, H.; Goeppert, A.; Prakash, G. K. S.; Olah, G. Applicability of Linear Polyethylenimine Supported on Nano-Silica for the Adsorption of CO2 from Various Sources Including Dry Air. *RSC Adv.* **2015**, *5*, 52550−52562.
(50) Planas, N.; Dzubak, A. L.; Poloni, R.; Lin, L. C.; McManus, A.; McDonald, T. M.; Neaton, J. B.; Long, J. R.; Smit, B.; Gagliardi, L. The Mechanism of Carbon Dioxide Adsorption in an Alkylamine-Functionalized Metal-Organic Framework. *J. Am. Chem. Soc.* **2013**, *135*, 7402−7405.

DOI: 10.1021/acsami.7b02471
ACS Appl. Mater. Interfaces 2017, 9, 11299−11306